Synthesis and photocatalytic property of Cu_2CoSnS_4 nanocrystals with stannite and wurtzite structure

Hao Guan ✉, *Xiao Ma, Jia Zhao*

School of Materials Science and Engineering, Yancheng Institute of Technology, 9 Yinbing Street, Yancheng 224051, People's Republic of China
✉ *E-mail: guanhao1980@sina.com*

Published in Micro & Nano Letters; Received on 19th September 2019; Revised on 19th December 2019; Accepted on 2nd January 2020

Stannite and wurtzite Cu_2CoSnS_4 (CCTS) nanocrystals are successfully prepared via a solvothermal approach. X-ray diffraction and Raman spectroscopy reveal that pure CCTS phases with stannite and wurtzite structure are obtained. Scanning electron microscopy shows that CCTS nanocrystals with stannite structure are composed of nanosheets with the thickness of about 50 nm while CCTS nanocrystals with wurtzite structure exhibit large number of irregular nanoparticles. Furthermore, photoluminescence (PL) spectroscopy and UV–Vis spectroscopy are used to investigate optical and photocatalytic properties of CCTS nanocrystals. When CCTS nanocrystals with stannite and wurtzite structure are used as photocatalysts, the degradation of methylene blue can reach up to 72 and 53%, respectively, within 100 min under visible-light irradiation, which are suitable for effective visible-light photocatalysts.

1. Introduction: Recently, with the development of industrialisation, water pollution has become a severe worldwide problem. Developing new environmentally-friendly technologies to treat the pollutants has attracted interest of many researchers. Some materials, especially semiconductors, have been applied to degrade organic contaminants under sunlight irradiation [1]. As an important quaternary chalcogenide semiconductor for solar energy conversion, Cu_2ZnSnS_4 (CZTS) containing earth-abundant, non-toxic and low-cost elements has been proven a good photovoltaic and photocatalytic material owing to its direct bandgap energy around 1.5 eV and high absorption coefficient. We believe that Cu_2CoSnS_4 (CCTS) is also considered as another alternative for treatment of organic contaminants owing to its similar structure to CZTS. However, As far as we all know, CCTS has never been studied as photocatalytic material. To date, CCTS compounds have been synthesised by some approaches [2–16]. Compared with other methods, the solvothermal approach has some advantages, such as small grain sizes and easier operation. To the best of our knowledge, no reports have been found to synthesise wurtzite CCTS nanocrystals by a solvothermal approach.

Herein, CCTS nanocrystals with stannite and wurtzite structure are successfully synthesised via a solvothermal approach, and their structures, morphologies, optical and photocatalytic properties are studied by different characterisation tools.

2. Experimental details: Copper nitrate trihydrate ($Cu(NO_3)_2{\cdot}3H_2O$, 99%), cobaltous acetate tetrahydrate ($Co(CH_3COO)_2{\cdot}4H_2O$, 99.5%), tin(Π) chloride dihydrate ($SnCl_2{\cdot}2H_2O$, 98%) and thiourea (H_2NCSNH_2, 99%) are used as received. In a typical experiment, the precursor solutions were prepared by dissolving 0.025M $Cu(NO_3)_2{\cdot}3H_2O$, 0.0125M $Co(CH_3COO)_2{\cdot}4H_2O$, 0.0125M $SnCl_2{\cdot}2H_2O$ and 0.05M H_2NCSNH_2 in 40 ml ethylene glycol and ethylenediamine (EDA), respectively. Then the precursor solutions are transferred into autoclaves and kept for 12 h at 200°C. After cooled to room temperature, the samples are obtained by being centrifuged at 8000 rpm for 3 min and washed several times with deionised water. Finally, the samples are dried at 80°C for 3 h in vacuum for further use.

In a photocatalytic experiment, 50 mg CCTS is added into 50 ml methylene blue (MB) solution of 10^{-5} mol/l. Before the solutions are exposed to visible light irradiation, which are continuous stirred for 30 min in the dark to set up adsorption–desorption equilibrium. Approximately 5 ml solution from the as-obtained reactor at given time intervals is used as measured solutions after CCTS nanocrystals are separated from the liquid by centrifugation.

The crystal phases are studied by X-ray diffraction (XRD, PaNalytical X'Pert Pro) and Raman spectroscopy (JY-T64000). The morphologies are investigated by scanning electron microscope (LEO-1530VP). The photoluminescence (PL) spectra are recorded by luminescence spectrometer (PerkinElmer LS-55). The optical and photocatalytic properties are measured by spectrophotometer (Shimadzu UV-2450).

3. Results and discussion: Fig. 1 shows the XRD patterns of as-obtained CCTS nanocrystals in different solvents. It is clearly revealed that the diffraction patterns of stannite and wurtzite CCTS structures are shown, peaks at 2θ values of 28.7°, 47.6° and 56.7° correspond to (112), (204) and (312) planes of stannite CCTS, respectively. While peaks at 2θ values of 27.1°, 28.6°, 30.8°, 47.7°, 51.9° and 56.4° are assigned to (100), (002), (101), (110), (103) and (112) planes of wurtzite CCTS, respectively. The XRD patterns of two samples with broad peaks illustrate the existence of CCTS nanocrystals. The average crystallite size of CCTS nanocrystals with stannite and wurtzite structure using Debye-Scherrer formula can be calculated to be about 7.2 and 15.2 nm, respectively. We all know that the small difference of the total energy between stannite and wurtzite cannot rule out the possible formation of CCTS with wurtzite structure. Therefore, metastable wurtzite CCTS structure can be obtained through a kinetic-controlled process with the adjustment of the coordination properties of the solvent and reaction temperature. When EDA is used as solvent, wurtzite CCTS phase can be formed owing to the reduction of the surface energy being caused by the robust chelating ability of EDA along with relatively lower synthesis temperature (200°C). The phenomenon is similar to the one reported in the literature [17, 18].

In addition to the XRD, the as-obtained CCTS nanocrystals in different solvents are further characterised by Raman spectroscopy since XRD does not clearly distinguish the difference between CCTS and Cu_2SnS_3 due to the similarity of their structure. As can be seen in Fig. 2, two strong peaks at 335 and 330 cm^{-1} attributed to stannite and wurtzite CCTS phases are observed, respectively, which are in good agreement with experimental data in the literature [19]. There are no Raman peaks of Cu_2SnS_3

doi: 10.1049/mnl.2019.0583

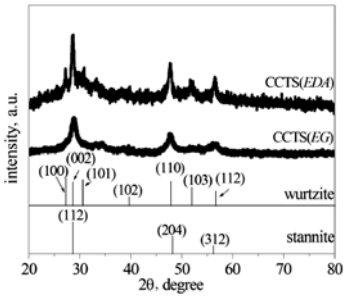

Fig. 1 *XRD patterns of the Cu_2CoSnS_4 nanocrystals with stannite and wurtzite structure*

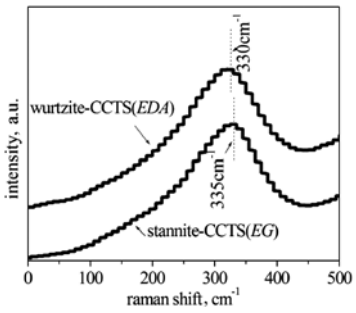

Fig. 2 *Raman spectra of the Cu_2CoSnS_4 nanocrystals with stannite and wurtzite structure*

(290, 318 and 348 cm^{-1}) are found, which demonstrates that the single-phase CCTS with stannite and wurtzite structures are synthesised.

Fig. 3 shows that scanning electron microscopy (SEM) images of as-obtained CCTS nanocrystals in different solvents. We can see that stannite CCTS nanocrystals display nanosheet morphology and rough surface, and the thickness of small nanocrystals with the grain size is ~15 nm. Compared with stannite CCTS nanocrystals, wurtzite CCTS nanocrystals exhibit large number of irregular nanoparticles with an average size ~18 nm. In the solvothermal process, the solvent plays an essential role in the formation of CCTS particles with different morphologies. It can be explained that CCTS nanosheets are formed through anisotropic growth while the irregular CCTS nanoparticles are obtained through isotropic growth.

It is well known that the optical characteristic is more important for photocatalyst. The optical bandgaps of as-obtained CCTS nanocrystals in different solvents can be determined by plotting $(\alpha h\nu)^2$ against $h\nu$. The bandgaps of stannite CCTS phase and wurtzite CCTS phase are determined to be 1.43 and 1.49 eV, respectively, as shown in Fig. 4, implying the usage of full spectrum of visible light for good photocatalytic activities. The measured bandgap values are shift from bulk CCTS ($E_g = 1.5$ eV). This shift is discussed to be highly possible due to the quantum confinement

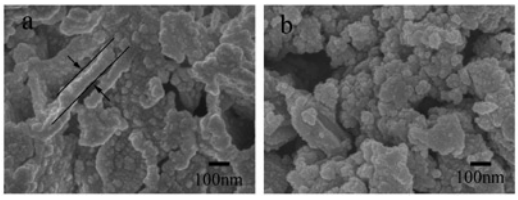

Fig. 3 *SEM images of the Cu_2CoSnS_4 nanocrystals with different structures*
a SEM image of the Cu_2CoSnS_4 nanocrystals with stannite structure
b SEM image of the Cu_2CoSnS_4 nanocrystals with wurtzite structure

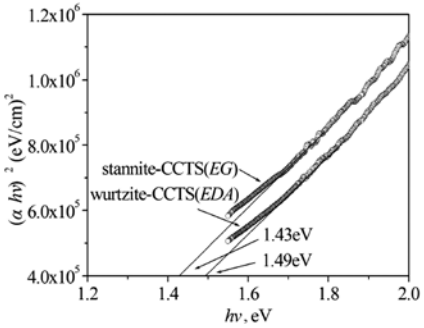

Fig. 4 *Optical bandgap estimations of the Cu_2CoSnS_4 nanocrystals with stannite and wurtzite structure*

effect of CCTS nanocrystals [20, 21]. Moreover, the bandgap of stannite CCTS phase is lower than that of wurtzite CCTS phase, showing that stannite CCTS phase can apparently enhance the MB degradation rate by expanding photo-response ability to visible light.

For semiconductors, the PL spectra can be used to investigate the migration, transfer and recombination processes of photo-generated charge carriers [22, 23]. Fig. 5 shows the PL spectra of as-obtained CCTS nanocrystals in different solvents. It is observed that the PL intensity of stannite CCTS phase is lower than that of wurtzite CCTS phase, indicating that stannite CCTS phase has a lower recombination rate between photo-generated electrons and holes and thus a corresponding higher photocatalytic property.

As we all know, the photocatalytic reaction is caused by the creation of hole–electron pairs. When the MB solution with the addition of CCTS nanocrystals is irradiated, generation of hole–electron of CCTS semiconductor takes place. The hole charge carriers react with H_2O or OH^- to produce hydroxyl radical groups (•OH). In addition, the electron charge carriers react with O_2 and H_2O to produce •OH. Further, The MB dye can be discoloured owing to additional species obtained by reaction between •OH and MB dye. Fig. 6 shows possible schematic mechanism. In order to prove the photocatalytic ability, CCTS

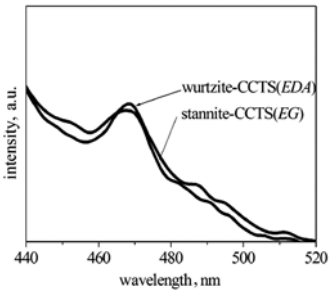

Fig. 5 *PL spectra of the Cu_2CoSnS_4 nanocrystals with stannite and wurtzite structure*

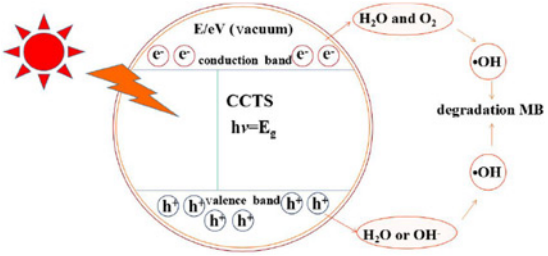

Fig. 6 *Basic mechanism of photocatalytic reactions of Cu_2CoSnS_4 catalysts*

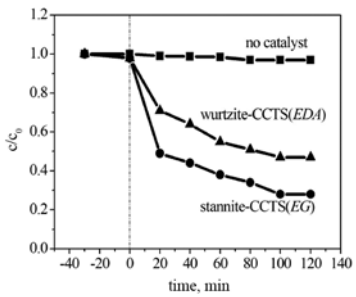

Fig. 7 *Degradation rates of MB as a function of different time with and without Cu_2CoSnS_4 nanocrystals under visible light*

nanocrystals are examined for the degradation of MB under visible-light irradiation. Fig. 7 shows the photocatalytic degradation rates (C/C_0) under visible-light irradiation. After 100 min visible-light irradiation, the concentration of MB shows almost no change in the absence of CCTS, indicating that MB does not spontaneously undergo the photocatalytic degradation under visible-light irradiation. The degradation rates of MB with the addition of CCTS nanocrystals with stannite and wurtzite structure are about 72 and 53%, respectively, under 100 min visible-light irradiation. Moreover, compared with wurtzite CCTS nanocrystals, stannite CCTS nanocrystals exhibit higher photocatalytic activity because of larger surface areas of CCTS nanosheets. Based on the above research, we propose that CCTS can be used as visible-light photocatalyst.

4. Conclusions: In summary, CCTS nanocrystals with stannite and wurtzite structure are successfully prepared via a solvothermal approach. The solvent plays a virtual role in the formation and morphologies of two different CCTS phases. Under 100 min visible-light irradiation, CCTS nanocrystals with stannite and wurtzite structure can lead to about 72 and 53% discolouration for the MB, respectively. The study demonstrates that CCTS is a promising alternative for visible-light photocatalyst.

5 References

[1] Zheng Y., Pan Z.M., Wang X.C: 'Advances in photocatalysis in China', *Chin. J. Catal.*, 2013, **34**, pp. 524–535

[2] Zhang X.Y., Bao N.Z., Lin B.P., *ET AL.*: 'Colloidal synthesis of wurtzite Cu_2CoSnS_4 nanocrystals and the photoresponse of spray-deposited thin films', *Nanotechnol.*, 2013, **24**, p. 105706

[3] Chane-Ching J.Y., Gillorin A., Zaberca O., *ET AL.*: 'Highly-crystallized quaternary chalcopyrite nanocrystalsvia a high-temperature dissolution reprecipitation route', *Chem. Commun.*, 2011, **47**, pp. 5229–5231

[4] Murali B., Krupanidhi S.B.: 'Facile synthesis of Cu_2CoSnS_4 nanoparticles exhibiting red-edge-effect: application in hybrid photonic devices', *J. Appl. Phys.*, 2013, **114**, p. 144312

[5] Zaberca O., Gillorin A., Durand B., *ET AL.*: 'A general route to the synthesis of surfactant-free, solvent-dispersible ternary and quaternary chalcogenide nanocrystals', *J. Mater. Chem.*, 2011, **21**, pp. 6483–6486

[6] Zhong J., Wang Q., Cai W.: 'Rapid synthesis of flower-like Cu_2CoSnS_4 microspheres with nanoplates using a biomolecule-assisted method', *Mater. Lett.*, 2015, **150**, pp. 69–72

[7] Cui Y., Deng R., Wang G., *ET AL.*: 'A general strategy for synthesis of quaternary semiconductor Cu_2MSnS_4 (M=Co^{2+}, Fe^{2+}, Ni^{2+}, Mn^{2+}) nanocrystals', *J. Mater. Chem.*, 2012, **22**, pp. 23136–23140

[8] Ozel F., Aslan E., Istanbullu B., *ET AL.*: 'Photocatalytic hydrogen evolution based on Cu_2ZnSnS_4, Cu_2NiSnS_4 and Cu_2CoSnS_4 nanocrystals', *Appl. Catal. B, Environ.*, 2016, **198**, pp. 67–73

[9] Ozel F.: 'Earth-abundant quaternary semiconductor Cu_2MSnS_4 (M=Fe, Co, Ni and Mn) nanofibers: fabrication, characterization and band gap arrangement', *J. Alloy Compd.*, 2016, **657**, pp. 157–162

[10] Krishnaiah M., Mishra R.K., Seo S.G., *ET AL.*: 'Annealing temperature and stabilizer effects on morphological evolution of Cu_2CoSnS_4 films on thermally oxidized Si wafers via direct spin-coating', *J. Alloy Compd.*, 2019, **781**, pp. 1091–1100

[11] Sarilmaz A., Ozel F.: 'Synthesis of band-gap tunable earth-abundant CXTS (X=Mn^{2+}, Co^{2+}, Ni^{2+} and Zn^{2+}) nanorods: toward a generalized synthesis strategy of quaternary chalcogenides', *J. Alloy Compd.*, 2019, **780**, pp. 518–522

[12] Wang T., Zhan Q., Cheng W.: 'Synthesis and characterization of Cu_2CoSnS_4 thin films prepared via radio-frequency (RF) magnetron sputtering', *J. Mater. Sci., Mater. Electron.*, 2019, **30**, pp. 2285–2291

[13] Ghediya Prashant R., Chaudhuri Tapas K.: 'Dip-coated Cu_2CoSnS_4 thin films from molecular ink for solar photovoltaics', *Mater. Res. Express*, 2018, **5**, p.085509

[14] Maldar P.S., Mane A.A., Nikam S.S.: 'Temperature dependent properties of spray deposited Cu_2CoSnS_4 (CCTS) thin films', *J. Mater. Sci., Mater. Electron.*, 2017, **28**, pp. 18891–18896

[15] Maldar P.S., Gaikwad M.A., Mane A.A.: 'Fabrication of Cu_2CoSnS_4 thin films by a facile spray pyrolysis for photovoltaic application', *Sol. Energy*, 2017, **158**, pp. 89–99

[16] Xie Y., Zhang C., Yang G.: 'Highly crystalline stannite-phase Cu_2XSnS_4 (X = Mn, Fe, Co, Ni, Zn and Cd) nanoflower counter electrodes for ZnO-based dye-sensitised solar cells', *J. Alloy Compd.*, 2017, **696**, pp. 938–946

[17] Bahramzadeh S., Abdizadeh H., Golobostanfard M.R.: 'Controlling the morphology and properties of solvothermal synthesized Cu_2ZnSnS_4 nanoparticles by solvent type', *J. Alloy Compd.*, 2015, **642**, pp. 124–130

[18] Hou H., Guan H., Li L.: 'Synthesis of Cu_2FeSnS_4 thin films with stannite and wurtzite structure directly on glass substrates via the solvothermal method', *J. Mater. Sci., Mater. Electron.*, 2017, **28**, pp. 7745–7748

[19] Guan H., Wang X., Huang Y.: 'Optical, photocatalytic and thermoelectric properties of Cu_2MeSnS_4 (Me = Mn^{2+}, Fe^{2+}, Co^{2+}) nanocrystals via microwave-assisted solvothermal method', *Chalcogenide Lett.*, 2018, **15**, pp. 435–440

[20] Su Z., Yan C., Tang D., *ET AL.*: 'Fabrication of Cu_2ZnSnS_4 nanowires and nanotubes based on AAO templates', *Cryst. Eng. Commun.*, 2012, **14**, pp. 782–785

[21] Gillorin A., Balocchi A., Marie X., *ET AL.*: 'Synthesis and optical properties of Cu_2CoSnS_4 colloidal quantum dots', *J. Mater. Chem.*, 2011, **21**, pp. 5615–5619

[22] Liu H., Cao W.R., Su Y., *ET AL.*: 'Bismuth oxyiodide-graphene nanocomposites with high visible light photocatalytic activity', *J. Colloid Interface Sci.*, 2013, **398**, pp. 161–167

[23] Yu C.L., Yu J.C., Fan C.F., *ET AL.*: 'Synthesis and characterization of Pt/BiOI nanoplate catalyst with enhanced activity under visible light irradiation', *Mater. Sci. Eng. B*, 2010, **166**, pp. 213–219

doi: 10.1049/mnl.2019.0583